

MODULATIONS OF VISCOUS FLUID CONDUIT PERIODIC WAVES

MICHELLE D. MAIDEN, MARK A. HOEFER

Department of Applied Mathematics, University of Colorado, Boulder, CO

ABSTRACT. In this work, modulation of periodic interfacial waves on a conduit of viscous liquid is explored utilizing Whitham theory and Nonlinear Schrödinger (NLS) theory. Large amplitude periodic wave modulation theory does not require integrability of the underlying model equation, yet in practice, either integrable equations are studied or the full extent of Whitham (wave-averaging) theory is not developed. The governing conduit equation is nonlocal with nonlinear dispersion and is not integrable. Via a scaling symmetry, periodic waves can be characterized by their wavenumber and amplitude. In the weakly nonlinear regime, both the defocusing and focusing variants of the NLS equation are derived, depending on the wavenumber. Dark and bright envelope solitons are found to persist in the conduit equation. Due to non-convex dispersion, modulational instability for periodic waves above a critical wavenumber is predicted. In the large amplitude regime, structural properties of the Whitham modulation equations are computed, including strict hyperbolicity, genuine nonlinearity, and linear degeneracy. Bifurcating from the NLS critical wavenumber at zero amplitude is an amplitude-dependent elliptic region for the Whitham equations within which a maximally unstable periodic wave is identified. These results have implications for dispersive shock waves, recently observed experimentally.

1. INTRODUCTION

Nonlinear wave modulation is a major mathematical component of the description of dispersive hydrodynamics. Dispersive hydrodynamics encompasses the study of fluid-like media where dissipative effects are weak compared to dispersion [6]. Solitary waves and dispersive shock waves (DSWs) are typical coherent structures. Model equations include the integrable Korteweg-de Vries (KdV) and Nonlinear Schrödinger (NLS) equations as well as non-integrable counterparts that are important for applications to superfluids, geophysical fluids, and laser light. Modulation theory assumes the existence of a multi-parameter family of nonlinear, periodic traveling wave solutions whose parameters change slowly relative to the wavelength and period of the periodic solution under perturbation. Such variation is described by modulation equations. In the weakly nonlinear regime, the NLS equation is a universal model for the slowly varying envelope, incorporating both cubic nonlinearity and dispersion. In the large amplitude regime, the Whitham equations [45] describe slow modulations of the wave's mean, amplitude, and wavenumber. At leading order, they are a dispersionless system of quasi-linear equations.

In this paper, we investigate nonlinear wave modulations in both the weakly nonlinear and large amplitude regimes for the conduit equation

$$(1) \quad A_t + (A^2)_z - (A^2(A^{-1}A_t)_z)_z = 0.$$

This equation approximately governs the evolution of the circular interface, with cross-sectional area A , separating a light, viscous fluid rising buoyantly through a heavy, more viscous, miscible fluid at small Reynolds numbers [32, 20]. Our motivation for studying eq. (1) is two-fold. First, the conduit equation is not integrable [13] so there are mathematical challenges in analyzing its rich variety of nonlinear wave features. Second, equation (1) is an accurate model of viscous fluid conduit interfacial waves where hallmark experiments have been performed on solitary waves [29, 42, 14], their interactions [32, 43, 21], and DSWs [23]. We believe the conduit system is an ideal model for the study of a broad range of dispersive hydrodynamic phenomena. Indeed, in this work we elucidate additional nonlinear wave phenomena predicted by eq. (1) by analyzing the weakly nonlinear, NLS reduction and by examining the structural properties of the large

E-mail address: michelle.maiden@colorado.edu, hoefer@colorado.edu.

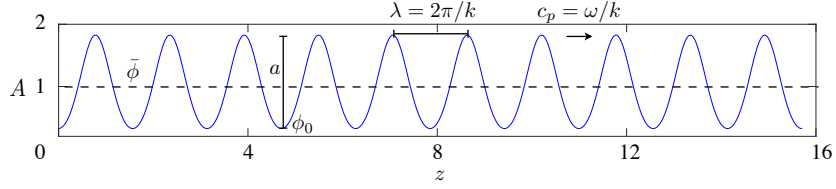


FIGURE 1. Example of a periodic wave solution to the conduit equation with wavenumber $k = 2$, amplitude $a = 1.5$, and unit mean.

amplitude modulation (Whitham) equations. We use these equations to study properties of modulated periodic wave solutions of the conduit equation, an example of which is shown in Fig. 1

1.1. Background on viscous fluid conduits. Conduits generated by the low Reynolds number, buoyant dynamics of two miscible fluids with differing densities and viscosities were first studied in the context of geological and geophysical processes [40]. A system of equations describing the dynamics of melted rock within a solid rock matrix was derived by treating molten rock and its solid, porous surroundings as two fluids with a large density and viscosity difference [26]. Under appropriate assumptions, the family of magma equations

$$(2) \quad \varphi_t + (\varphi^n)_x - (\varphi^n (\varphi^{-m} \varphi_t)_x)_x = 0$$

describing the evolution of the volume fraction φ of melted rock, can be derived [30, 35]. There are two constitutive model parameters (n, m) that relate the porosity of the rock matrix to its permeability and viscosity, respectively. The conduit equation (1) is precisely the magma equation (2) when $(n, m) = (2, 1)$ [32]. Viscous fluid conduits, in contrast to magma, are easily accessible in a laboratory setting, typically with a sugar solution or glycerine for the exterior fluid, and a dyed, diluted version of one of these fluids for the interior fluid [29, 32, 43, 23].

Early experiments primarily explored the development of the conduit itself, which results in a diapir followed by a periodic wavetrain [40, 29]. Solitary waves in the established conduit have also been extensively studied, including their amplitude-speed relation, interactions, and fluid transport properties [29, 32, 42, 14, 21]. Experiments have also shown that interactions between solitons are nearly elastic, with a phase shift the primary quantifiable change [14, 21]. Furthermore, soliton interaction geometries predicted by Lax for the KdV equation [17] were observed and agreed well with numerical simulations [21]. Recently, dispersive shock waves (DSWs) were observed, yielding good agreement with predictions from Whitham averaging theory [23]. The accompanying observations of soliton-DSW interaction suggest a high degree of coherence, i.e., the sustenance of dissipationless/dispersive hydrodynamics over long spatial and temporal time scales. It is for this reason that we further investigate modulations of periodic conduit waves.

1.2. Properties of the conduit equation. To fully describe the two-fluid interface of the conduit system, one can consider the full Navier-Stokes equations with boundary conditions along a moving, free interface. However, in the small interfacial slope, long-wave regime, a balance between the viscous stress force of the exterior fluid and the buoyancy force acting on the interior fluid leads to the asymptotically resolved conduit equation (1) with no amplitude assumption [29, 20]. The force balance is achieved with small interfacial slopes on the order of the square root of the ratio of the interior to exterior fluid viscosities.

The conduit equation (1) has been studied since the 1980s. The equation has exactly two conservation laws [2, 12]:

$$(3) \quad \begin{cases} A_t + (A_2 - A^2(A_{-1}A_t)_z)_z &= 0, \\ \left(\frac{1}{A} + \frac{A_z^2}{A^2}\right)_t + \left(\frac{A_{tz}}{A} - \frac{A_z A_t}{A^2} - 2 \ln A\right)_z &= 0. \end{cases}$$

The conduit equation itself corresponds to conservation of mass and obeys the scaling invariance

$$(4) \quad \tilde{A} = A/A_0, \quad \tilde{z} = A_0^{-1/2} z, \quad \tilde{t} = A_0^{1/2} t.$$

The linearization of the conduit equation upon a unit area background admits trigonometric traveling wave solutions subject to the frequency dispersion relation

$$(5) \quad \omega_0(k) = \frac{2k}{1+k^2},$$

with wavenumber k . This leads to the linear phase c_p and group c_g velocities

$$(6) \quad c_p(k) = \frac{\omega_0(k)}{k} = \frac{2}{1+k^2}, \quad c_g(k) = \omega'_0(k) = \frac{2(1-k^2)}{1+k^2}.$$

Note that $c_g < c_p$ for $k > 0$. While the phase velocity is always positive, the group velocity is negative for $k > 1$. Failure of the Painlevé test suggests that the conduit equation is not completely integrable [13]. The conduit equation is globally well-posed for initial data $A(\cdot, 0) - 1 \in H^1(\mathbb{R})$ with $A(z, 0)$ physically-relevant initial data bounded away from zero in order to avoid the singularity [34].

Solitary waves have been studied numerically for the more general magma equation (2) where it has been found that solitary waves exhibit near-elastic interactions resulting in a phase-shift and a physically negligible dispersive tail [31, 27, 21]. The asymptotic stability of solitary waves has also been proven [33]. General (unmodulated) periodic wave solutions have been found, and an implicit dispersion relation has been computed for these waves [29]. In the long wavelength, small amplitude regime, the conduit equation reduces to KdV [41].

There have been several works applying periodic traveling wave modulation theory to the magma equations (2). Reference [25] considered Eq. (2) with $(n, m) = (3, 0)$, describing DSWs and structural properties of the Whitham equations. Modulations of periodic traveling waves in the magma equation (2) and a generalization of it were investigated in the weakly nonlinear, KdV regime [10]. Modulated periodic waves in the form of DSWs were investigated for the entire family of magma equations (2) in [19].

1.3. Outline of this work. The paper is organized as follows. Periodic traveling wave solutions to the conduit equation are studied in Sec. 2 both numerically and asymptotically in the weakly nonlinear regime. In Sec. 3, we consider weakly nonlinear periodic wave modulations and include long wave dispersion to derive the NLS equation. By an appropriate choice of the periodic traveling wave's wavenumber, both the focusing and defocusing variants of the NLS equation are possible. We numerically demonstrate the persistence of dark and bright modulation solitary wave solutions in the full conduit equation. In Sec. 4, we analyze modulated periodic waves of arbitrary amplitude via the conduit Whitham modulation equations. By weakly nonlinear analysis and direct numerical computation, we determine structural properties of the Whitham equations including hyperbolicity or ellipticity and genuine nonlinearity or linear degeneracy. The manuscript is concluded with a discussion of the implications of this work in Section 5.

2. PERIODIC TRAVELING WAVE SOLUTIONS

We seek periodic traveling wave solutions to Eq. (1) in the form $A(z, t) = \phi(\theta)$, $\theta = kz - \omega t$, $\phi(\theta + 2\pi) = \phi(\theta)$ for $\theta \in \mathbb{R}$. Inserting this ansatz into Eq. (1) yields

$$(7) \quad -\omega\phi' + k(\phi^2)' + \omega k^2(\phi^2(\phi^{-1}\phi')')' = 0.$$

Integrating twice results in

$$(8) \quad (\phi')^2 = g(\phi) \equiv -\frac{2}{k^2}\phi - \frac{2}{\omega k}\phi^2 \ln \phi + A + B\phi^2,$$

where A and B are real integration constants.

Equation (8) exhibits at most three real roots [19]. When there are three distinct roots, a periodic solution oscillates between the largest two. The solution can be parameterized by three independent variables. Defining the wave minimum ϕ_0 according to $\phi_0 = \min_\theta \phi(\theta)$, we utilize the following physical parametrization

$$(9) \quad \begin{aligned} \text{wavenumber:} & \quad k, \\ \text{wave amplitude:} & \quad a = \max_{\theta \in [0, \pi]} \phi(\theta) - \phi_0, \\ \text{wave mean:} & \quad \bar{\phi} \equiv \frac{1}{\pi} \int_0^\pi \phi(\theta) d\theta = \frac{1}{\pi} \int_{\phi_0}^{\phi_0+a} \frac{\phi d\phi}{\sqrt{g(\phi)}}. \end{aligned}$$

The requirement that ϕ is 2π -periodic is enforced through

$$(10) \quad \pi = \int_0^\pi d\theta = \int_{\phi_0}^{\phi_0+a} \frac{d\phi}{\sqrt{g(\phi)}},$$

where in (9) and (10) we have used the even symmetry of solutions to eq. (8). Given $(k, a, \bar{\phi})$, the relations (9) and (10) determine the wave frequency $\omega = \omega(k, a, \bar{\phi})$ and the wave minimum $\phi_0 = \phi_0(k, a, \bar{\phi})$. The extrema requirements $g(\phi_0) = g(\phi_0 + a) = 0$ determine A and B from Eq. (8).

Due to the scaling invariance Eq. (4), the wave mean can be scaled to unity. This implies that only $\omega(k, a, 1)$ and $\phi_0(k, a, 1)$ need be determined. Then the general cases follow according to

$$(11) \quad \omega(k, a, \bar{\phi}) = \bar{\phi}^{1/2} \omega(\bar{\phi}^{-1/2} k, \bar{\phi}^{-1} a, 1), \quad \phi_0(k, a, \bar{\phi}) = \bar{\phi} \phi_0(\bar{\phi}^{-1/2} k, \bar{\phi}^{-1} a, 1).$$

We therefore define the unit-mean dispersion and wave solution according to

$$(12) \quad \tilde{\omega}(\tilde{k}, \tilde{a}) = \omega(\tilde{k}, \tilde{a}, 1), \quad \tilde{\phi}(\theta; \tilde{k}, \tilde{a}) = \phi(\theta; \tilde{k}, \tilde{a}, 1).$$

We will use the variables $(\tilde{\phi}, \tilde{\omega}, \tilde{k}, \tilde{a})$ whenever we are assuming a unit mean solution.

2.1. Stokes expansion. We can obtain approximate periodic traveling wave solutions in the weakly nonlinear regime via the Stokes wave expansion [44]:

$$(13) \quad \tilde{\phi} = 1 + \varepsilon \tilde{\phi}_1 + \varepsilon^2 \tilde{\phi}_2 + \varepsilon^3 \tilde{\phi}_3 + \dots,$$

$$(14) \quad \tilde{\omega} = \tilde{\omega}_0 + \varepsilon^2 \tilde{\omega}_2 + \dots,$$

where $0 < \varepsilon \ll 1$ is an amplitude scale. Inserting this ansatz into Eq. (7), equating like coefficients in ε , and enforcing solvability conditions yields the approximate solution

$$(15) \quad \tilde{\phi}_1(\theta) = \cos \theta, \quad \tilde{\omega}_0(k) = \frac{2\tilde{k}}{1+\tilde{k}^2}, \quad \tilde{\phi}_2(\theta) = \frac{1}{6\tilde{k}\tilde{\omega}_0} \cos 2\theta, \quad \tilde{\omega}_2(\tilde{k}) = \frac{1-8\tilde{k}^2}{48\tilde{k}(1+\tilde{k}^2)},$$

where $\tilde{\omega}_0$ is the unit mean linear dispersion relation (5). Setting the amplitude $\tilde{a} = 2\varepsilon$, the approximate periodic wave solution is

$$(16) \quad \tilde{\phi}(\theta) = 1 + \frac{\tilde{a}}{2} \cos \theta + \frac{\tilde{a}^2(1+\tilde{k}^2)}{48\tilde{k}^2} \cos 2\theta + \mathcal{O}(\tilde{a}^3),$$

$$(17) \quad \tilde{\omega}(\tilde{k}, \tilde{a}) = \frac{2\tilde{k}}{1+\tilde{k}^2} + \tilde{a}^2 \frac{1-8\tilde{k}^2}{48\tilde{k}(1+\tilde{k}^2)} + \mathcal{O}(\tilde{a}^3).$$

In Fig 2, this solution is compared to numerically computed periodic waves (numerical methods are described in Appendix A.1). The frequency and wave profile of the Stokes expansion accurately describe some periodic conduit waves, even for $\mathcal{O}(1)$ amplitudes provided the wavenumber is appropriately chosen. However, even at moderately small wavenumbers, the expansion rapidly breaks down. This is quantified in Fig. 3. Figure 3(a,b) shows the dispersion and phase velocity for numerically computed periodic waves, and (c) compares the full, nonlinear dispersion $\tilde{\omega}(\tilde{k}, \tilde{a})$ to $\tilde{\omega}_0(\tilde{k}) + \tilde{a}^2 \tilde{\omega}_2(\tilde{k})$. Note the dispersion relation agrees exceedingly well for $\tilde{k} > 1$ and $\tilde{a} \lesssim 1$, but deviates for larger amplitudes and wavenumbers less than 0.5.

Of interest is that the approximate solution (16) can result in an unphysical, negative conduit cross-sectional area. The minimum of the approximate solution $\tilde{\phi}(\theta)$ occurs when $\theta = \pi$. Equating the minimum to zero, we find that physical, positive values for approximate $\tilde{\phi}$ are restricted to $\tilde{a} < a_0$, where $a_0 > 4(3 - \sqrt{6}) \approx 2.20$, which is well beyond our assumption of small amplitude $0 < \tilde{a} \ll 1$.

3. WEAKLY NONLINEAR, DISPERSIVE MODULATIONS

The aim of this section is to describe wave modulation in the weakly nonlinear regime. The approximate NLS equation is found using multiple scales in Appendix B by seeking a solution in the form

$$(18) \quad A(z, t) = 1 + \varepsilon [\sqrt{n} B e^{i\theta} + c.c.] + \varepsilon^2 \left[\frac{nB^2}{3\tilde{k}\tilde{\omega}_0} e^{2i\theta} + c.c. + M \right] + \mathcal{O}(\varepsilon^3),$$

$$M = \frac{(3\tilde{k} - 1)(1 + \tilde{k}^2)}{\tilde{k}^2(\tilde{k}^2 + 3)} n |B|^2, \quad n(\tilde{k}) = \frac{3 + 5\tilde{k}^2 + 8\tilde{k}^4}{3\tilde{k}(\tilde{k}^2 + 1)(\tilde{k}^2 + 3)}$$

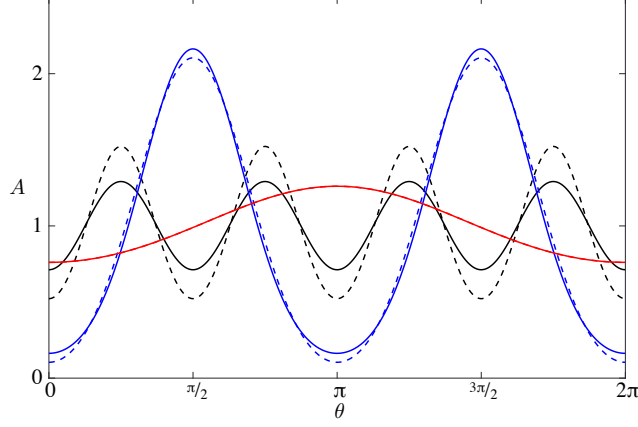


FIGURE 2. Comparison of the Stokes wave expansion solution (dashed lines) to the numerically computed solution (solid lines) for three different waves with unit mean. (k, a) is $(1/4, 1)$ (black), $(2, 2)$ (blue), and $(1, 0.5)$ (red).

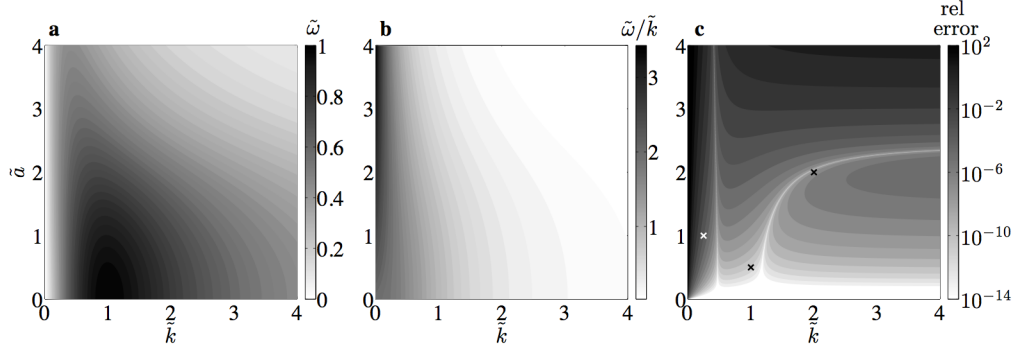


FIGURE 3. a) Contour plot of numerically computed dispersion relation. b) Numerically computed phase velocity. c) Relative error between numerically computed dispersion $\tilde{\omega}(\tilde{k}, \tilde{a})$ and approximate dispersion $\tilde{\omega}_0(\tilde{k}) + \tilde{a}^2 \tilde{\omega}_2(\tilde{k})$. Markers (x) correspond to waves plotted in Fig. 2.

where *c.c.* denotes complex conjugate and ε is an amplitude scale. By introducing the standard, scaled coordinate system

$$\tau = \varepsilon^2 t, \quad \zeta = \frac{\varepsilon}{\sqrt{|\tilde{\omega}_0''|}}(z - \tilde{\omega}_0' t),$$

we obtain the NLS equation for the complex envelope $B(\zeta, \tau)$

$$(19) \quad iB_\tau + \frac{\sigma}{2} B_{\zeta\zeta} + |B|^2 B = 0,$$

where $\sigma = \text{sgn} \tilde{\omega}_0''(\tilde{k})$ denotes the dispersion curvature. Since

$$\tilde{\omega}_0''(\tilde{k}) = \frac{4\tilde{k}(\tilde{k}^2 - 3)}{(1 + \tilde{k}^2)^3},$$

the NLS equation (19) is defocusing when $0 < \tilde{k} < \sqrt{3}$, and focusing for $\tilde{k} > \sqrt{3}$. This result effectively splits periodic wave solutions of the conduit equation into two regimes. For the defocusing case, weakly nonlinear periodic waves are modulationally stable, and dark envelope solitons are predicted, which, when combined

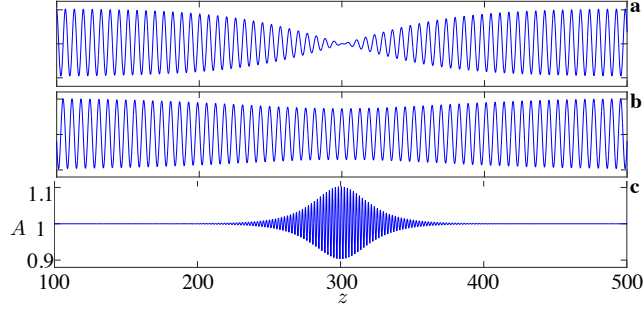


FIGURE 4. Examples of (a) black, (b) gray, and (c) bright envelope solitons from the NLS approximation. These approximate solutions were found to persist for the conduit equation over long time ($t = \mathcal{O}(1/\varepsilon^2)$), provided the modulated wave was of amplitude $\tilde{a} = 2\varepsilon \lesssim 0.4$. The pictured dark (bright) solitons are on a background wave with $\varepsilon = 0.1$ and $\tilde{k} = 1$ ($\tilde{k} = 3$). The gray soliton exhibits the phase jump $\alpha = \pi/4$.

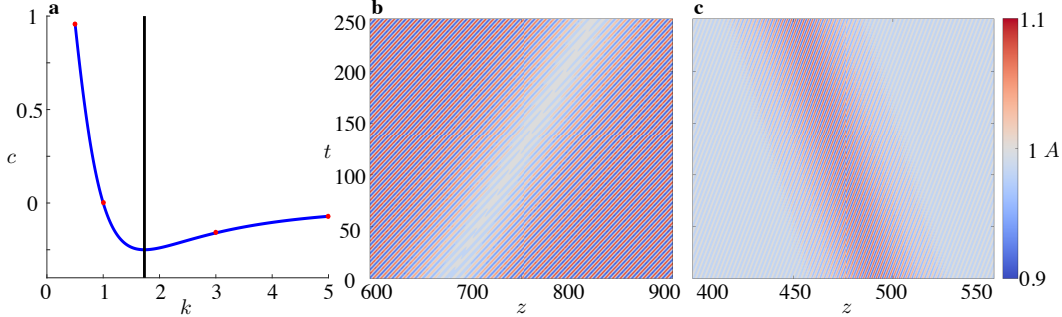


FIGURE 5. (a) Comparison of envelope soliton velocities extracted from numerical simulation (dots) to the linear group velocity (solid line). The vertical line denotes the crossover from defocusing to focusing NLS. (b,c) Contour plots of dark (b) and bright (c) envelope solitons. The dark (bright) soliton modulates a periodic wave with $\varepsilon = 0.05$ and $\tilde{k} = 0.5$ ($\tilde{k} = 3$).

with the ansatz (18), take the form (see, e.g., [1])

$$\text{(black)} \quad B(\zeta, \tau) = \tanh(\zeta) e^{i\tau},$$

$$\text{(gray)} \quad B(\zeta, \tau) = e^{2i\tau + i\psi_0} [\cos \alpha + i \sin \alpha \tanh[\sin \alpha (\zeta - 2 \cos \alpha \tau - \zeta_0)]] ,$$

with arbitrary, real constants ζ_0 , ψ_0 , and α , where α is the phase jump across the gray soliton. Examples of modulated periodic waves in this regime are shown in Figs. 4(a,b). For the focusing case, periodic waves are modulationally unstable [48]. Bright envelope solitons are predicted, which have the form

$$\text{(bright)} \quad B(\zeta, \tau) = \text{sech}(\zeta - \zeta_0) e^{-i\Theta}, \quad \Theta = -2\tau + \Theta_0,$$

where ζ_0 and Θ_0 are arbitrary, real constants. An example of a bright envelope soliton is shown in Fig. 4(c).

We find that approximate bright and dark envelope solitons persist to times $t = \mathcal{O}(1/\varepsilon^2)$ by direct numerical simulation of the conduit equation (1) with envelope soliton initial data. Appendix A.2 describes our numerical time-stepping method. The evolution of a black and a bright envelope soliton is depicted in the contour plots of Fig. 5. While the black soliton Fig 5(a) propagates forward in time, the bright soliton 5(b) has a negative velocity.

The velocity of both the dark and bright approximate envelope solitons are, to leading order in ε , the group velocity Eq. (5). We find excellent agreement between the predicted group velocity and the velocity extracted from numerical simulation as shown in Fig. 5(a). Envelope solitons, dark or bright, for $\tilde{k} > 1$ exhibit negative velocity.

For simulation times sufficiently large, $t \gg 1/\varepsilon^2$, envelope solitons emit radiation. The dark soliton decays and the bright soliton decomposes into smaller wave packets. We also find that numerical simulation of envelope solitons modulating periodic waves of sufficiently large amplitude ($\varepsilon \gtrsim 0.1$) breakdown almost immediately, although some dark envelope solitons appear to asymptote to a stable but different envelope form. Due to the breakdown of the NLS approximation at finite amplitudes, we require a more accurate description of nonlinear wave modulations in the moderate to large amplitude regime.

4. WHITHAM EQUATIONS

In order to describe modulated, large amplitude periodic waves, we appeal to the Whitham modulation equations. Whitham's original formulation invoked averaged conservation laws [46], later shown to be equivalent to a perturbative, multiple-scales reduction [22]. For completeness, we have implemented the multiple-scales reduction in Appendix C. For this, we seek modulations of an arbitrary amplitude, 2π -periodic, traveling wave solution ϕ to eq. (1) (see Sec. 2). Since we will incorporate only the leading order Whitham equations, the large parameter $1/\varepsilon$ here corresponds to the time scale of their validity. Note that this is shorter than the $\mathcal{O}(1/\varepsilon^2)$ time scale of the NLS equation (19). Then we arrive at the Whitham equations (Appendix C)

$$(20) \quad \begin{aligned} (\overline{\phi})_t + (\overline{\phi^2} - 2k\omega\overline{g(\phi)})_z &= 0, \\ \left(\frac{1}{\phi} + k^2 \frac{\overline{g(\phi)}}{\phi^2} \right)_t - 2(\overline{\ln \phi})_z &= 0, \\ k_t + \omega_z &= 0, \end{aligned}$$

where we recall the defining ordinary differential equation (ODE) $\phi'^2 = g(\phi)$ (8) and utilize the notation

$$\bar{f} = \frac{1}{2\pi} \int_0^{2\pi} f(\theta) d\theta.$$

It is convenient to express the Whitham equations in the form

$$(21) \quad \mathcal{P}_t + \mathcal{Q}_z = 0, \quad \mathcal{P} = \begin{bmatrix} \overline{\phi} \\ I_1 \\ k \end{bmatrix}, \quad \mathcal{Q} = \begin{bmatrix} I_2 \\ I_3 \\ \omega \end{bmatrix},$$

where we have introduced the averaging integrals

$$(22) \quad I_1 = \overline{\phi^{-1}} + k^2 \overline{g(\phi)/\phi^2}, \quad I_2 = \overline{\phi^2} - 2k\omega\overline{g(\phi)}, \quad I_3 = -2\overline{\ln \phi}.$$

Furthermore, we can expand the density \mathcal{P} and flux \mathcal{Q} in terms of the modulation variables $\mathbf{q} = (k, a, \overline{\phi})^T$ to obtain the quasi-linear form of the Whitham equations

$$(23) \quad \mathbf{q}_t + \mathcal{A}\mathbf{q}_z = 0,$$

where

$$(24) \quad \mathcal{A} = \left(\frac{\partial \mathcal{P}}{\partial \mathbf{q}} \right)^{-1} \frac{\partial \mathcal{Q}}{\partial \mathbf{q}} = \begin{bmatrix} \frac{\omega_k}{I_{3,k} - I_{1,k}\omega_k - I_{2,k}I_{1,\overline{\phi}}} & \frac{\omega_a}{I_{3,a} - I_{1,k}\omega_a - I_{2,a}I_{1,\overline{\phi}}} & \frac{\omega_{\overline{\phi}}}{I_{3,\overline{\phi}} - I_{1,k}\omega_{\overline{\phi}} - I_{2,\overline{\phi}}I_{1,\overline{\phi}}} \\ \frac{I_{1,a}}{I_{2,k}} & \frac{I_{1,a}}{I_{2,a}} & \frac{I_{1,a}}{I_{2,\overline{\phi}}} \end{bmatrix}.$$

This non-conservative form of the Whitham equations is only valid where the matrix $\partial \mathcal{P}/\partial \mathbf{q}$ is invertible.

The scaling invariance (4) can be used so that the dependence on $\overline{\phi}$ in the Whitham equations is explicit and the averaging integrals need be computed only over the scaled variables \tilde{k} and \tilde{a} . Then the integrals (22) can be written

$$(25) \quad I_1 = \frac{1}{\overline{\phi}} \tilde{I}_1, \quad I_2 = \overline{\phi}^2 \tilde{I}_2, \quad I_3 = \tilde{I}_3 - 2 \ln \overline{\phi},$$

where $\tilde{I}_i = \tilde{I}_i(\tilde{k}, \tilde{a})$, $i = 1, 2, 3$. Therefore, computation of the averaging integrals is only required for (\tilde{k}, \tilde{a}) . The Whitham equations in the scaled variables $\tilde{\mathbf{q}} = (\tilde{k}, \tilde{a}, \bar{\phi})$ are

$$(26) \quad \tilde{\mathbf{q}}_t + \tilde{\mathcal{A}}\tilde{\mathbf{q}}_z = 0, \quad \tilde{\mathcal{A}} = \left(\frac{\partial \mathbf{q}}{\partial \tilde{\mathbf{q}}}\right)^{-1} \mathcal{A} \frac{\partial \mathbf{q}}{\partial \tilde{\mathbf{q}}}, \quad \frac{\partial \mathbf{q}}{\partial \tilde{\mathbf{q}}} = \begin{bmatrix} \bar{\phi}^{-1/2} & 0 & -\frac{1}{2}\bar{\phi}^{-3/2}\tilde{k} \\ 0 & \bar{\phi} & \tilde{a} \\ 0 & 0 & 1 \end{bmatrix}.$$

We will be interested in structural properties of the Whitham equations such as hyperbolicity (strict or non-strict), ellipticity, and genuine nonlinearity. All of these criteria rely on the eigenvalues and eigenvectors of the Whitham equations that satisfy

$$(27) \quad (\mathcal{A} - cI)\mathbf{r} = 0.$$

In general, we expect three eigenpairs $\{(c_j, \mathbf{r}_j)\}_{j=1}^3$ with either all real eigenvalues $c_1 \leq c_2 \leq c_3$, where the Whitham equations are hyperbolic. If the inequalities are strict, then the Whitham equations are strictly hyperbolic. Or, in the case of one real and two complex conjugate eigenvalues, the Whitham equations are elliptic.

The coefficient matrix $\tilde{\mathcal{A}}$ is a similarity transformation of \mathcal{A} so its eigenvalues are the same. $\tilde{\mathcal{A}}$ exhibits the following property

$$(28) \quad \tilde{\mathcal{A}}(\tilde{k}, \tilde{a}, \bar{\phi}) = \begin{bmatrix} 1 & 0 & 0 \\ 0 & 1 & 0 \\ 0 & 0 & \bar{\phi} \end{bmatrix} \tilde{\mathcal{A}}(\tilde{k}, \tilde{a}, 1) \begin{bmatrix} \bar{\phi} & 0 & 0 \\ 0 & \bar{\phi} & 0 \\ 0 & 0 & 1 \end{bmatrix},$$

which can be used to show

$$(29) \quad c(\tilde{k}, \tilde{a}, \bar{\phi}) = \bar{\phi}c(\tilde{k}, \tilde{a}, 1), \quad \mathbf{r}(\tilde{k}, \tilde{a}, \bar{\phi}) = \begin{bmatrix} \bar{\phi}^{-1} & 0 & 0 \\ 0 & \bar{\phi}^{-1} & 0 \\ 0 & 0 & 1 \end{bmatrix} \mathbf{r}(\tilde{k}, \tilde{a}, 1).$$

Therefore, the hyperbolicity/ellipticity of the Whitham equations is independent of the mean $\bar{\phi}$. We define the unit mean eigenvalues \tilde{c} and eigenvectors $\tilde{\mathbf{r}}$ according to

$$(30) \quad \tilde{c}(\tilde{k}, \tilde{a}) = c(\tilde{k}, \tilde{a}, 1), \quad \tilde{\mathbf{r}}(\tilde{k}, \tilde{a}) = \mathbf{r}(\tilde{k}, \tilde{a}, 1).$$

Utilizing the identities in (29), we find that the quantity

$$(31) \quad \mu \equiv \nabla_{\tilde{\mathbf{q}}} c(\tilde{k}, \tilde{a}, \bar{\phi}) \cdot \mathbf{r}(\tilde{k}, \tilde{a}, \bar{\phi}) = \begin{bmatrix} \tilde{c}_{\tilde{k}} \\ \tilde{c}_{\tilde{a}} \\ \tilde{c} \end{bmatrix} \cdot \tilde{\mathbf{r}}$$

is independent of $\bar{\phi}$, $\mu = \mu(\tilde{k}, \tilde{a})$. If $\mu \neq 0$, then the Whitham equations are genuinely nonlinear [45]. For those values of \tilde{k} and \tilde{a} where $\mu = 0$, the Whitham equations are linearly degenerate. The sign definiteness of μ corresponds to a monotonicity condition that is required for the existence of simple wave solutions to the Whitham equations, of particular importance for the study of DSWs [6].

4.1. Weakly nonlinear regime. We now consider Eq. (24) in the small a regime by inserting the Stokes expansion (16), (17), yielding

$$(32) \quad \mathcal{A} = \begin{bmatrix} \omega_{0,k} & 2a\omega_2 & \frac{\omega_{0,\bar{\phi}}}{2} \\ \frac{a}{2}\omega_{0,kk} & \omega_{0,k} & \frac{a}{2} \frac{4(1+\bar{\phi}k^2+3\bar{\phi}^2k^4+\bar{\phi}^3k^6)}{(1+\bar{\phi}k^2)^3} \\ 0 & 2a \frac{1-3\bar{\phi}k^2}{8(1+\bar{\phi}k^2)} & \frac{2\bar{\phi}}{2\bar{\phi}} \end{bmatrix} + \mathcal{O}(a^2).$$

We directly compute the characteristic velocities and, via (29), evaluate at unit mean $\bar{\phi} = 1$

$$(33) \quad \begin{aligned} \tilde{c}_1 &= \tilde{\omega}_{0,\tilde{k}} - \frac{\tilde{a}}{4} \sqrt{-n\tilde{\omega}_{0,\tilde{k}\tilde{k}}} + \mathcal{O}(\tilde{a}^2), \\ \tilde{c}_2 &= \tilde{\omega}_{0,\tilde{k}} + \frac{\tilde{a}}{4} \sqrt{-n\tilde{\omega}_{0,\tilde{k}\tilde{k}}} + \mathcal{O}(\tilde{a}^2), \\ \tilde{c}_3 &= 2 + \mathcal{O}(\tilde{a}^2), \end{aligned}$$

where $n = n(\tilde{k})$ is from Eq. (18). We observe that complex characteristic velocities occur precisely when the NLS equation (19) is in the focusing regime, i.e., when $\tilde{k} > \sqrt{3}$. This is to be expected [45]. The requirement $-\tilde{n}\tilde{\omega}_{0,\tilde{k}\tilde{k}} > 0$ for modulational stability is sometimes referred to as the Benjamin-Feir-Lighthill criterion [48]. Note that we must use $-n(\tilde{k})$, as opposed to $\tilde{\omega}_2(\tilde{k})$ from the Stokes expansion (15), in the criterion because of the generation of a mean term (cf. [45]).

Because the linear group velocity (6) is always less than the linear, long wave velocity 2, the weakly nonlinear approximation of the Whitham equations imply strict hyperbolicity $\tilde{c}_1 < \tilde{c}_2 < \tilde{c}_3$ for $\tilde{a} > 0$, $\tilde{k}^2 < 3$.

Next, we determine the approximate eigenvectors $\tilde{\mathbf{r}}_i$ associated with the approximate eigenvalues (33) using standard asymptotics of eigenvalues and eigenvalues (see, e.g., [15]). These approximate results are used to compute μ_i , $i = 1, 2, 3$ (31). The expressions are cumbersome but there are two noteworthy findings. We find that $\mu_1 = 0$ when

$$(34) \quad \tilde{a} = 6\sqrt{\frac{2}{5}}3^{3/4}(\sqrt{3} - \tilde{k})^{3/2} + \mathcal{O}\left((\sqrt{3} - \tilde{k})^{5/2}\right), \quad 0 < \sqrt{3} - \tilde{k} \ll 1.$$

Along the curve (34), the weakly nonlinear Whitham equations are linearly degenerate in the first characteristic field.

We also find linear degeneracy in the second characteristic field: $\mu_2 = 0$ when $\tilde{a} = 18\tilde{k}^2 + \mathcal{O}(\tilde{k}^4)$, $0 < \tilde{k} \ll 1$. But the weakly nonlinear Whitham equations are nonstrictly hyperbolic, $\tilde{c}_2 = \tilde{c}_3$, when $\tilde{a} = 12\tilde{k}^2 + \mathcal{O}(\tilde{k}^4)$, $0 < \tilde{k} \ll 1$. Because nonstrict hyperbolicity implies linear degeneracy [4], we have apparently obtained a contradiction. We argue that this is due to the asymptotic approximations made and the poor accuracy of the approximate periodic wave solution afforded by the Stokes expansion (16), (17) for small \tilde{k} (cf. Figs. 2, 3).

4.2. Large amplitude regime. We now investigate modulations of large amplitude, periodic waves by direct computation of the Whitham equations. For this, we examine the Whitham equations in the form (26), so that the dependence on $\bar{\phi}$ is explicit. We numerically compute periodic solutions $\bar{\phi}$ and the corresponding dispersion $\tilde{\omega}(\tilde{k}, \tilde{a})$ and unit-mean averaging integrals $\{\tilde{I}_i(\tilde{k}, \tilde{a})\}_{i=1}^3$ for the equispaced, discrete values $(\tilde{k}_j, \tilde{a}_l)$, $\tilde{k}_j = j\Delta$, $\tilde{a}_l = l\Delta$, $j, l = 1, 2, \dots, N$. We chose $N = 4000$, $\Delta = 0.001$ so that $\tilde{k}_N = \tilde{a}_N = 4$. Derivatives of $\tilde{\omega}$ and \tilde{I}_j with respect to \tilde{k} and \tilde{a} , required in (23), are estimated with sixth order finite differences, yielding a numerical approximation of the coefficient matrix $\tilde{\mathbf{A}}$ on the discrete grid.

Using our direct computation of the coefficient matrix $\tilde{\mathbf{A}}$, we determine its eigenvalues $\{\tilde{c}_i(\tilde{k}, \tilde{a})\}_{i=1}^3$ and plot in Fig. 6a the region in the \tilde{k} - \tilde{a} plane where the Whitham equations are hyperbolic or elliptic. As shown by our weakly nonlinear analysis (33), the elliptic region appears for $\tilde{k} > \sqrt{3}$, independent of \tilde{a} for small \tilde{a} . But our computations show that the region depends strongly on the wave amplitude.

As noted earlier, ellipticity of the Whitham equations implies modulational instability of the periodic traveling wave [48]. In agreement with our weakly nonlinear analysis (33), we find that in the elliptic region, $\tilde{c}_1 = \tilde{c}_2^*$ (* denotes complex conjugation) and $\tilde{c}_3 \in \mathbb{R}$. We confirm the hyperbolic/elliptic boundary by direct numerical simulation of the conduit equation (1) with slightly perturbed, periodic initial data. Random, smooth noise (band-limited to wavenumber 512) of magnitude $\mathcal{O}(10^{-3})$ was added to a periodic traveling wave initial condition on a domain of over 100 spatial periods. This initial data was evolved either 100 temporal periods or to $t = 500$, whichever was longer. Some waves, especially those in the small-amplitude regime, were evolved for even longer time periods. The modulational (in)stability of several of these runs are shown in Fig. 6(a). We find excellent agreement with the MI predictions from Whitham theory. The long-time evolution of two particular waves are shown in Fig. 7, showing both a stable and an unstable case.

A periodic traveling wave solution of the conduit equation (1) corresponds to a constant solution $\tilde{\mathbf{q}}(z, t) = \tilde{\mathbf{q}}_0$ of the Whitham equations (26). If we consider the stability of this solution by linearizing the Whitham equations according to $\tilde{\mathbf{q}}(z, t) = \tilde{\mathbf{q}}_0 + \mathbf{b}e^{i\kappa z + \sigma t}$, $|\mathbf{b}| \ll 1$, we obtain the growth rates

$$(35) \quad \sigma_i = \kappa \text{Im}(c_i),$$

for each component of the perturbation in the eigenvector basis of $\tilde{\mathbf{A}}$. The physical growth rate requires knowledge of the wavenumber κ . Because the Whitham equations are quasi-linear, first order equations, any wavenumber is permissible (determined by the initial data), suggesting that the physical growth rate (35) is unbounded. In practice, there is a dominant wavenumber associated with the instability that is determined

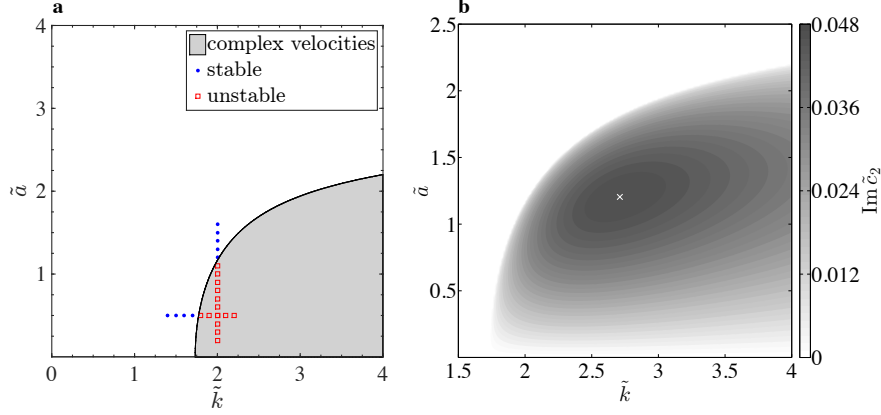


FIGURE 6. a) Elliptic (gray) and hyperbolic (white) parameter regimes for the Whitham equations corresponding to complex or real characteristic velocities, respectively. Stable (dots) and unstable (squares) periodic waves according to direct numerical simulation of the conduit equation. b) Contour plot of the imaginary part of the characteristic velocity \tilde{c}_2 , the MI growth rate. The maximum, 0.04795, occurs for $(\tilde{k}, \tilde{a}) = (2.711, 1.204)$.

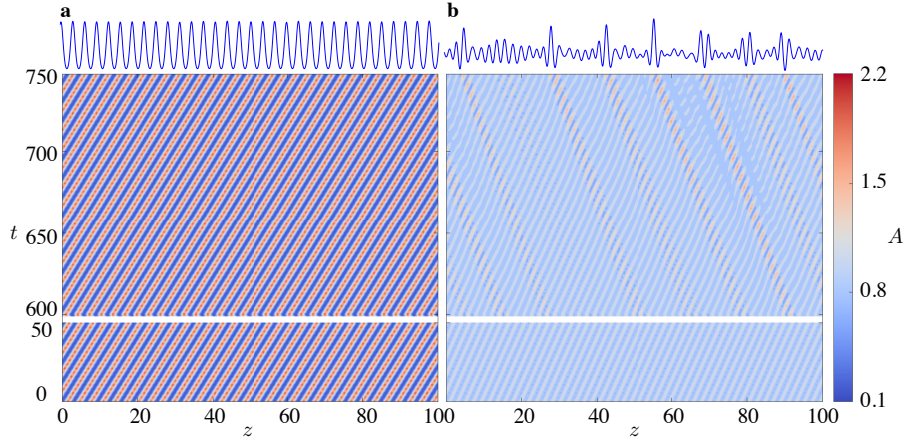


FIGURE 7. Numerical evolution of perturbed periodic wave solutions in the conduit equation. a) Modulationally stable case: $(\tilde{k}, \tilde{a}) = (2, 2)$. b) Modulationally unstable case: $(\tilde{k}, \tilde{a}) = (3, 0.5)$. Top: the respective cases at the final time $t = 750$.

by higher order effects, which in this case is dispersion. The NLS equation (19) resolves this feature in the weakly nonlinear regime but we are interested in large amplitude modulations. We therefore identify the imaginary part of the characteristic velocity \tilde{c}_2 as a proxy for the growth rate of the instability and observe in Fig. 6b that there is a maximum of $\text{Im}(\tilde{c}_2)$ for unit-mean periodic waves that occurs for the wave parameters $(\tilde{k}, \tilde{a}) = (2.711, 1.204)$. We confirm that these parameters do indeed approximately correspond to a maximally unstable periodic wave by performing numerical simulations of the conduit equation (1) with initially perturbed periodic traveling waves, using the same process used when determining modulational (in)stability. The envelopes of these waves were extracted for each time step and then compared to the envelope of the initial condition, giving a deviation from the expected periodic wave evolution. The growth rate was calculated by fitting an exponential to this deviation. From these numerics, the maximally unstable parameters are closer to $(\tilde{k}, \tilde{a}) = (2.7, 1.35)$ than the expected $(\tilde{k}, \tilde{a}) = (2.7, 1.2)$. The maximal growth rate for these parameters was found to be 0.0457, which is within 5% of the maximal growth rate found via the Whitham equations. Thus the κ does not drastically affect the maximal growth rates.

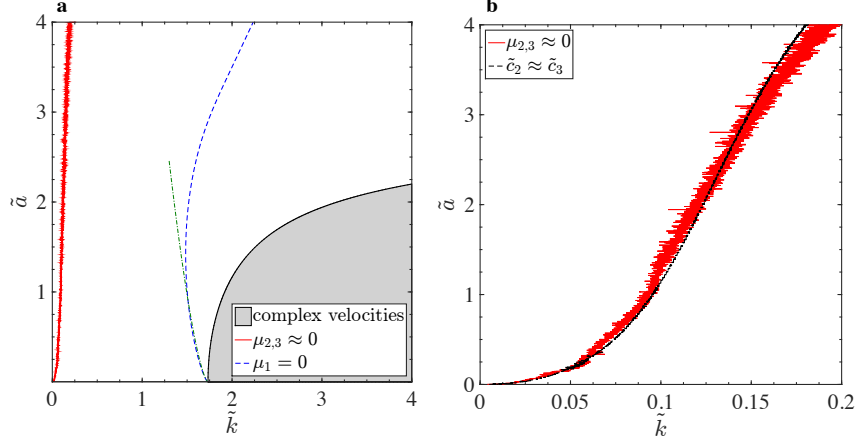


FIGURE 8. a) Loss of genuine nonlinearity in the Whitham equations. The curves correspond to regions in the \tilde{k} - \tilde{a} plane where the computed quantities $\mu_{2,3}$ (solid) or μ_1 (dashed) change sign. To the right of the solid (dashed) curve, $\mu_3 > 0$, $\mu_2 < 0$ ($\mu_1 > 0$). The dash-dotted curve corresponds to the prediction $\mu_1 = 0$ from a weakly nonlinear analysis. The elliptic region from Fig. 6 is also depicted (gray). b) Zoom-in of the small \tilde{k} region of a) where $\mu_{2,3} \approx 0$ (red) approximately corresponds to the largest \tilde{k} , to the left of which $|\tilde{c}_3 - \tilde{c}_2| < 10^{-5}$ (black), i.e., approaching non-strict hyperbolicity.

Next, we compute the quantities $\{\mu_i(\tilde{k}, \tilde{a})\}_{i=1}^3$ from eq. (31) on the discrete grid $\{(\tilde{k}_j, \tilde{a}_l)\}_{j,l=1}^N$ using sixth order finite differencing. The results are depicted in Fig. 8a where the curves correspond to the largest value of \tilde{k} , given \tilde{a} , such that μ changes sign. The curve where μ_1 changes sign bifurcates from the edge of the elliptic region at the point $(\tilde{k}, \tilde{a}) = (\sqrt{3}, 0)$, agreeing with the weakly nonlinear result (34) for sufficiently small \tilde{a} . The curve where both $\mu_{2,3}$ change sign apparently bifurcates from $(0, 0)$ and occurs for small \tilde{k} . These results demonstrate that the Whitham equations lack genuine nonlinearity when considered in the whole of the hyperbolic region.

In order to understand the small \tilde{k} results better, we show in Fig. 8b a zoom-in of this region. The accurate determination of the loss of genuine nonlinearity in this region is numerically challenging because the characteristic velocities $\tilde{c}_{2,3}$ get very close to one another. A more numerically stable calculation is shown by the black dashed curve in Fig. 8b where, for each \tilde{a} , it corresponds to the largest \tilde{k} at which $|\tilde{c}_3 - \tilde{c}_2| < 10^{-5}$. For parameters to the left of this curve, the characteristic velocities remain very close to one another. It is well-known that, for example, in the KdV Whitham equations, the characteristic velocities get exponentially close to one another yet remain distinct in the small wavenumber regime [18, 11]. Because non-strict hyperbolicity implies loss of genuine nonlinearity [4], the proximity of \tilde{c}_2 and \tilde{c}_3 may be affecting the numerical results. It remains to definitively determine if the Whitham equations lose strict hyperbolicity and/or genuine nonlinearity in the small \tilde{k} regime. Note that the curve for which $\mu_1 = 0$ in Fig. 8a occurs in a strictly hyperbolic region.

5. DISCUSSION/CONCLUSION

Our study of the structural properties of the conduit Whitham equations sheds some light on recent theoretical and experimental studies of dispersive shock waves. The DSW fitting method allows one to determine a dispersive shock's harmonic and soliton edge speeds, even for non-integrable systems [9]. However, the method is known to break down when the Whitham equations lose genuine nonlinearity in the second characteristic field [19, 6]. It was observed in [19] that the fitting method failed to accurately predict conduit DSW soliton edge speeds for sufficiently large jump heights. Our results here suggest that this could be due to the loss of strict hyperbolicity and/or genuine nonlinearity in the small wavenumber (soliton train) regime.

In addition to the hyperbolic modulation regime where DSWs, and dark envelope solitons are the prominent coherent structures, we have found an elliptic regime where the periodic wave breaks up into coherent

wavepackets or bright envelope solitons. The accessibility of both hyperbolic and elliptic modulation regimes in one system motivates further study of each and the transition between the two. One potential future, novel direction is to explore the possibility of creating a soliton gas [7].

It remains to generate a periodic wave from an initially constant conduit and explore its properties experimentally. Accurate control of wavebreaking has been achieved by slow modulation of the conduit area from a boundary [23]. One possibility is to utilize simple wave solutions of the Whitham equations to efficiently and smoothly transition between a constant conduit $\tilde{a} = 0$ to a periodic conduit $\tilde{a} > 0$. This also suggests the theoretical and experimental exploration of Riemann problems, step initial data, for the Whitham equations themselves. Our determination of linearly degenerate curves will inform the ability to construct simple waves connecting two generic wave states.

Although our direct numerical simulations suggest that envelope solitons are long-lived, their physical realization may be challenging. Existing laboratory studies of viscous fluid conduits implement control of the conduit interface by varying the injected flow rate through a nozzle at the bottom of a fluid column. This allows for the creation of waves with positive (upward) propagation velocities. While some dark solitons have a positive velocity, all bright envelope solitons propagate with negative velocity. Additionally, it has been found to be difficult to image small amplitude excitations so that the observation of weakly nonlinear dynamics may be challenging. Nevertheless, the experimental creation of periodic conduit waves and envelope solitons is possible.

We have shown that the non-convexity of the conduit linear dispersion relation leads to the existence of elliptic Whitham equations and modulational instability. This is just one possible implication of non-convex dispersion in dispersive hydrodynamics. We note that non-convex dispersion in other, higher order equations, has also been found to give rise to a resonance between the DSW soliton edge and linear waves, leading to the generation of radiating DSWs [3, 8, 38].

This study has identified and categorized modulations of periodic traveling waves for the conduit equation (1). These findings, along with previous theoretical and experimental studies of solitons and DSWs imply that the viscous fluid conduit system is an accessible environment in which to investigate rich and diverse nonlinear wave phenomena.

APPENDIX A. NUMERICAL METHODS

A.1. Periodic solutions. We compute unit-mean conduit periodic traveling wave solutions $\tilde{\phi}(\theta)$ for specified (\tilde{k}, \tilde{a}) with a Newton-GMRES iterative method [16] on the first integral of equation (7)

$$(36) \quad A + \tilde{\omega}\tilde{\phi} - \tilde{k}\tilde{\phi}^2 - \tilde{\omega}\tilde{k}^2\tilde{\phi}\tilde{\phi}'' + \tilde{\omega}\tilde{k}^2(\tilde{\phi}')^2 = 0,$$

where $A \in \mathbb{R}$ is an integration constant. We use a spectral method to compute the unit-mean cosine series representation $\tilde{\phi}(\theta) = 1 + \sum_{n=1}^N 2a_n \cos n\theta$. Equation (36) is discretized in spectral space $\{a_n\}_{n=1}^N$ with the fast and accurate computation of derivatives achieved via fast cosine transforms (DCT II in [39]). The projection of (36) onto constants determines A , which we do not require because of our imposition of unit mean. Projection of Eq. (36) onto $\cos(n\theta)$ for $n = 1, \dots, N$ yields N equations for the $N + 1$ unknowns $((a_n)_{n=1}^N, \tilde{\omega})$. The amplitude constraint $\tilde{\phi}(\pi) - \tilde{\phi}(0) = -4 \sum_{n \text{ odd}} a_n = \tilde{a}$ closes the system of equations. We precondition the spectral equations by dividing each by the sum of linear coefficients, shifted by $2k + 1$, i.e., by $\tilde{\omega} + n^2\tilde{\omega}\tilde{k}^2 + 1$. The accurate resolution of each solution is maintained by achieving an absolute tolerance of 10^{-13} in the 2-norm of the residual and choosing N so that $|a_n|$ is below $5 \cdot 10^{-12}$ for $n > 3N/4$. The number of coefficients required strongly depends on the wavenumber \tilde{k} . For example, when $0.5 \leq \tilde{k} \leq 4$, we find $N = 2^6$ provides sufficient accuracy whereas for $0.002 \leq \tilde{k} \leq 0.01$, we use $N = 2^{12}$.

With the cosine series coefficients of $\tilde{\phi}(\theta)$ in hand, we compute the unit-mean averaging integrals \tilde{I}_j , $j = 1, 2, 3$ in Eqs. (25), (22) using the spectrally accurate trapezoidal rule. We then use sixth order finite differencing to compute derivatives of \tilde{I}_j and $\tilde{\omega}$ on a grid of wavenumbers and amplitudes as explained in Sec. 4.2. This numerically determines the Whitham equations in the form (26).

A.2. Time stepping. For the direct numerical simulation of the conduit equation (1), it is convenient to write it in the form of two coupled equations:

$$(37) \quad \begin{cases} \mathcal{P} = A^{-1}A_t, \\ A\mathcal{P} + (A^2)_z - (A^2\mathcal{P}_z)_z = 0. \end{cases}$$

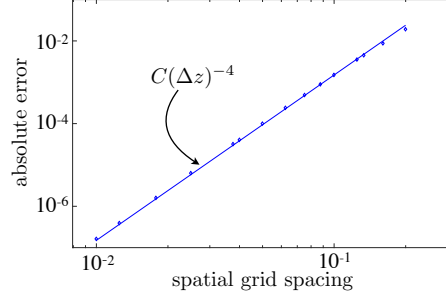


FIGURE 9. Maximum absolute error in the direct numerical simulation of the conduit equation, achieving fourth order spatial accuracy as expected. The solution used in validation was a periodic wave with $k = 3$ and $a = 0.5$ generated with accuracy 10^{-8} , and was simulated over 50 spatial periods and 5 temporal periods. The reference line is $C(\Delta z)^{-4}$.

The first equation is a temporal ODE in time and the second equation is a linear, elliptic problem $\mathcal{L}(A)\mathcal{P} = -(A^2)_z$ in space. We solve for \mathcal{P} using an equispaced fourth-order finite difference discretization and direct inversion of the resulting banded linear system. We implement time-dependent boundary conditions with prescribed $A(0, t)$ and $A(L, t)$ so that the first equation in (37) yields the boundary conditions for \mathcal{P} . Time-stepping is achieved with a fourth-order, explicit Runge-Kutta method with variable timestep (MATLAB's ode45). The solver was validated against computed periodic traveling wave solutions. The maximum error between the numerical solution and the periodic traveling wave solution is reported in Figure 9.

APPENDIX B. NONLINEAR SCHRÖDINGER EQUATION DERIVATION

Here, we derive an approximation of wave modulations in the small-amplitude, weakly nonlinear regime. Consider the ansatz

$$(38) \quad u(z, t) = 1 + \varepsilon u_0 + \varepsilon^2 u_1 + \varepsilon^3 u_2 + \dots, \quad \varepsilon \rightarrow 0,$$

where $u_i = u_i(\theta, Z, T)$ for $i = 0, 1, \dots$, $\theta = \tilde{k}z - \tilde{\omega}_0(\tilde{k})t$, $Z = \varepsilon z$, and $T = \varepsilon t$, where $\tilde{\omega}_0(\tilde{k})$ is the linear dispersion relation (5) for unit mean. Then, at $\mathcal{O}(\varepsilon)$, we obtain a linear, homogeneous equation for u_0

$$(39) \quad \mathcal{L}u_0 := -\omega u_{0,\theta} + 2ku_{0,\theta} + k^2 \omega u_{0,3\theta} = 0,$$

with solution $u_0 = \psi(Z, T)e^{i\theta} + c.c.$ where $c.c.$ denotes the complex conjugate of the previous terms. At $\mathcal{O}(\varepsilon^2)$, $\mathcal{L}u_1 = F_1$ where

$$F_1 = e^{2i\theta} [-2i\tilde{k}\psi^2] + e^{i\theta} [-\psi_T - \tilde{k}^2\psi_T - 2\psi_Z + 2\tilde{k}\tilde{\omega}_0\psi_Z] + c.c.$$

Solvability therefore implies $-(1 + \tilde{k}^2)[\psi_T + \tilde{\omega}'_0(k)\psi_Z] \sim \varepsilon g_1 + \dots$, where we have introduced the higher order correction g_1 . Solving for u_1 , we include second harmonic and mean terms $u_1 = \psi^2(Z, T)e^{2i\theta}/(3\tilde{k}\tilde{\omega}) + c.c + M(Z, T)$ with M to be determined at the next order. Solvability with respect to constants at $\mathcal{O}(\varepsilon^3)$ yields

$$M = \frac{(3\tilde{k} - 1)(1 + \tilde{k}^2)}{\tilde{k}^2(\tilde{k}^2 + 3)} |\psi|^2.$$

Solvability with respect to the first harmonic yields g_1 , which, upon entering the moving reference frame and scaling to long time

$$\xi = Z - \tilde{\omega}'_0 T, \tau = \varepsilon T,$$

yields the Nonlinear Schrödinger equation in the form

$$(40) \quad i\psi_\tau + \frac{\tilde{\omega}''(\tilde{k})}{2} \psi_{\xi\xi} + \frac{3 + 5\tilde{k}^2 + 8\tilde{k}^4}{3\tilde{k}(\tilde{k}^2 + 1)(\tilde{k}^2 + 3)} |\psi|^2 \psi = 0.$$

Appropriate scaling of ξ and ψ yields Eq. (19).

APPENDIX C. DERIVATION OF THE WHITHAM EQUATIONS

For completeness, we supply a synopsis of the multiple scales asymptotic derivation of the Whitham modulation equations. For the formal derivation here, we introduce slow space and time scales $Z = \varepsilon z$, $T = \varepsilon t$ and consider the ansatz

$$(41) \quad A(z, t) = u_0(\theta, Z, T) + \varepsilon u_1(\theta, Z, T) + \varepsilon^2 u_2(\theta, Z, T) + \cdots, \quad 0 < \varepsilon \ll 1,$$

where $\theta_z = k$ and $\theta_t = -\omega$. Continuity of mixed partials $\theta_{zt} = \theta_{tz}$ implies the conservation of waves

$$(42) \quad k_T + \omega_Z = 0,$$

one of the Whitham equations. We insert the ansatz (41) into the conduit equation (1) and equate like orders in ε . The $\mathcal{O}(1)$ equation is

$$(43) \quad -\omega u_{0,\theta} + 2k u_{0,\theta} u_{0,\theta} - k^2 \omega u_{0,\theta} u_{0,\theta\theta} + k^2 \omega u_{0,\theta} u_{0,3\theta} = 0.$$

Equation (43) is solved with a family of periodic traveling waves parameterized by $(k, a, \bar{\phi})$ (see Sec. 2) where the parameters are assumed to depend on the slow variables (Z, T) .

At the next order, $\mathcal{O}(\varepsilon)$, we obtain the linear problem $\mathcal{L}u_1 = f$ where

$$\begin{aligned} \mathcal{L}u_1 &= -\omega u_{1,\theta} + (-k^2 \omega u_{0,\theta} u_{1,\theta} + 2k u_{0,\theta} u_1)_\theta + k^2 \omega (u_{1,\theta\theta\theta} u_0 + u_{0,\theta\theta\theta} u_1), \\ f &= -u_{0,T} - k^2 u_{0,\theta\theta} u_{0,T} + k^2 u_{0,\theta} u_{0,\theta\theta T} - 2u_{0,\theta} u_{0,Z} + 2k \omega u_{0,\theta} u_{0,\theta Z} - 2k \omega u_{0,\theta} u_{0,\theta\theta Z}. \end{aligned}$$

There are two solvability conditions in the form $\langle w, f \rangle \equiv \int_0^{2\pi} w(\theta) f(\theta) d\theta = 0$, where $w \in \text{Ker } L^* = \text{span}\{1, u_0^{-2}\}$ for the the adjoint operator

$$\mathcal{L}^* w = \omega w_\theta + k^2 \omega [-(u_{0,\theta} w)_{\theta\theta} + (u_{0,\theta\theta} w)_\theta + u_{0,3\theta} w - (u_0 w)_{3\theta}] + 2k [u_{0,\theta} w - (u_0 w)_\theta],$$

with 2π -periodic boundary conditions. Note that there is a third, linearly independent function that is annihilated by \mathcal{L}^* , but it is not 2π -periodic. Applying the two solvability conditions $\langle 1, f \rangle = \langle u_0^{-2}, f \rangle = 0$, and adding Eq. (42), we arrive at the Whitham equations

$$(44) \quad (\bar{u}_0)_T + (\bar{u}_0^2 - 2k \omega \bar{u}_{0,\theta}^2)_Z = 0,$$

$$(45) \quad \left(\frac{1}{u_0} + k^2 \frac{\bar{u}_{0,\theta}^2}{u_0^2} \right)_T - 2 (\ln u_0)_Z = 0,$$

$$(46) \quad k_T + \omega_Z = 0$$

where $\bar{g} = \langle 1, g \rangle$. Setting $\varepsilon = 1$, i.e., considering the Whitham equations as the long time $t \gg 1$ asymptotic, we obtain Eqs. (20).

Averaging of the conservation laws (3) is achieved by inserting the ansatz $A(z, t) = \phi(\theta)$ and averaging the densities and fluxes over a period:

$$\begin{aligned} \bar{\phi}_t + \left(\phi^2 + \omega k \phi^2 (\phi^{-1} \phi_\theta)_\theta \right)_z &= 0, \\ \left(\frac{1}{\phi} + k^2 \frac{\phi_\theta^2}{\phi^2} \right)_t + \left(-\omega k \frac{\phi_{\theta\theta}}{\phi} + \omega k \frac{\phi_\theta \phi_{\theta\theta}}{\phi^2} - 2 \ln \phi \right)_z &= 0. \end{aligned}$$

Integration by parts and the addition of conservation of waves (42) yields the same set of Whitham equations (20).

REFERENCES

- [1] Ablowitz, M. J. 2011 *Nonlinear Dispersive Waves: Asymptotic Analysis and Solitons*. 1 edition. Cambridge, UK; New York: Cambridge University Press.
- [2] Barcilon, V. & Richter, F. M. 1986 Nonlinear Waves in Compacting Media. *J. Fluid Mech. Digital Archive* **164**, 429-448. (doi:10.1017/S0022112086002628)
- [3] Conforti, M., Baronio, F. & Trillo, S. 2014 Resonant radiation shed by dispersive shock waves. *Phys. Rev. A* **89**, 13807. (doi:10.1103/PhysRevA.89.013807)
- [4] Dafermos, C. M. 2009 *Hyperbolic Conservation Laws in Continuum Physics*. 3rd ed. Springer.
- [5] El, G. A., Grimshaw, R. H. J. & Smyth, N.F. 2008 Asymptotic description of solitary wave trains in fully nonlinear shallow-water theory. *Physica D* **19**, 2423-35.
- [6] El, G. A. & Hoefer, M. A. 2016 Dispersive shock waves and modulation theory. arXiv:1602.06163 [nlin.PS] .

- [7] El, G. A. & Kamchatnov, A. M. 2005 Kinetic Equation for a Dense Soliton Gas. *Phys. Rev. Lett.* **95**, 204101. (doi:10.1103/PhysRevLett.95.204101)
- [8] El, G. A. & Smyth, N. F. 2016 Radiating dispersive shock waves in non-local optical media. *Proc. R. Soc. A* **472**, 20150633. (doi:10.1098/rspa.2015.0633)
- [9] El, G. A. 2005 Resolution of a shock in hyperbolic systems modified by weak dispersion. *Chaos* **15**, 37103.
- [10] Elperin, T., Kleeorin, N. & Krylov, A. 1994 Nondissipative shock waves in two-phase flows. *Physica D* **74**, 372-385.
- [11] Gurevich, A. V., Krylov, A. L. & El, G. A. 1990 Nonlinear modulated waves in dispersive hydrodynamics. *Sov. Phys. JETP* **71**, 899-910.
- [12] Harris, S. 1996 Conservation laws for a nonlinear wave equation. *Nonlinearity* **9**, 187-208.
- [13] Harris, S. E. & Clarkson, P. A. 2006 Painleve analysis and similarity reductions for the magma equation. *SIGMA* **68**.
- [14] Helfrich, K. R. & Whitehead, J. A. 1990 Solitary waves on conduits of buoyant fluid in a more viscous fluid. *Geophys Astro Fluid* **51**, 35-52.
- [15] Hinch, E. G. 1991 *Perturbation Methods*. Cambridge, UK; New York: Cambridge University Press.
- [16] Kelley, C. T. 1995 *Iterative methods for linear and nonlinear equations*. Philadelphia: SIAM
- [17] Lax, P. D. 1968 Integrals of nonlinear equations of evolution and solitary waves. *Comm. Pur. Appl. Math.* **21**, 467-490.
- [18] Levermore, D. 1988 The hyperbolic nature of the zero dispersion KdV limit. *Commun Part Diff Eq* **13**, 495-514.
- [19] Lowman, N. K. & Hoefer, M. A. 2013 Dispersive shock waves in viscously deformable media. *J. Fluid Mech.* **718**, 524-557. (doi:10.1017/jfm.2012.628)
- [20] Lowman, N. K. & Hoefer, M. A. 2013 Dispersive hydrodynamics in viscous fluid conduits. *Phys. Rev. E* **88**, 23016. (doi:10.1103/PhysRevE.88.023016)
- [21] Lowman, N. K., Hoefer, M. A. & El, G. A. 2014 Interactions of large amplitude solitary waves in viscous fluid conduits. *J. Fluid Mech.* **750**, 372-384. (doi:10.1017/jfm.2014.273)
- [22] Luke, J. C. 1966 A perturbation method for nonlinear dispersive wave problems. *Proc. R. Soc. Lond. A* **292**, 403-412.
- [23] Maiden, M. D., Lowman, N. K., Anderson, D. V., Schubert, M. E. & Hoefer, M. A. 2016 Observation of Dispersive Shock Waves, Solitons, and Their Interactions in Viscous Fluid Conduits. *Phys. Rev. Lett.* **116**, 174501. (doi:10.1103/PhysRevLett.116.174501)
- [24] Marchant, T. R. & Smyth, N. F. 2005 Approximate solutions for magmon propagation from a reservoir. *IMA J Appl Math* **70**, 796-813.
- [25] Marchant, T. R. & Smyth, N. F. 2012 Approximate solutions for dispersive shock waves in nonlinear media. *J. Nonlinear Optic. Phys. Mat.* **21**, 18.
- [26] McKenzie, D. 1984 Generation and compaction of partially molten rock. *J Petrology* **25**, 713-765.
- [27] Nakayama, M. & Mason, D. P. 1991 Compressive solitary waves in compacting media. *Int J Nonlin Mech* **26**, 631-640. (doi:10.1016/0020-7462(91)90015-L)
- [28] Nakayama, M. & Mason, D. P. 1992 Rarefactive solitary waves in two-phase fluid flow of compacting media. *Wave Motion* **15**, 357-392. (doi:10.1016/0165-2125(92)90054-6)
- [29] Olson, P. & Christensen, U. 1986 Solitary Wave Propagation in a Fluid Conduit Within a Viscous Matrix. *J. Geophys. Res.* **91**, 6367-6374. (doi:10.1029/JB091iB06p06367)
- [30] Richter, F. M. & McKenzie, D. 1984 Dynamical Models for Melt Segregation from a Deformable Matrix. *J. Geol.* **92**, 729-740. (doi:10.1086/628908)
- [31] Scott, D. R. & Stevenson, D. J. 1984 Magma solitons. *Geophys. Res. Lett.* **11**, 1161-1164. (doi:10.1029/GL011i011p01161)
- [32] Scott, D. R., Stevenson, D. J. & Whitehead, J. A. 1986 Observations of solitary waves in a viscously deformable pipe. *Nature* **319**, 759-761. (doi:10.1038/319759a0)
- [33] Simpson, G. & Weinstein, M. 2008 Asymptotic stability of ascending solitary magma waves. *SIAM J. Math. Anal.* **40**, 1337-1391. (doi:10.1137/080712271)
- [34] Simpson, G., Spiegelman, M. & Weinstein, M. I. 2007 Degenerate dispersive equations arising in the study of magma dynamics. *Nonlinearity* **20**, 21-49. (doi:10.1088/0951-7715/20/1/003)
- [35] Simpson, G., Spiegelman, M. & Weinstein, M. I. 2010 A Multiscale Model of Partial Melts 1: Effective Equations. *J. Geophys. Res.* **115**, B04410.
- [36] Spiegelman, M. 1993 Flow in Deformable Porous Media. Part 2 Numerical Analysis - the Relationship Between Shock Waves and Solitary Waves. *J. Fluid Mech. Digital Archive* **247**, 39-63. (doi:10.1017/S0022112093000370)
- [37] Spiegelman, M. 1993 Flow in Deformable Porous Media. Part 1 Simple Analysis. *J. Fluid Mech. Digital Archive* **247**, 17-38. (doi:10.1017/S0022112093000369)
- [38] Sprenger, P. & Hoefer, M. A. 2016 Shock Waves in Non-Convex Dispersive Hydrodynamics. arXiv:1606.09229 [nlin.PS].
- [39] Wang, Z. & Hunt, B. R. 1985 The discrete W transform. *Appl. Math. Comput.* **16**, 19-48. (doi:10.1016/0096-3003(85)90008-6)
- [40] Whitehead, J. A. & Luther, D. S. 1975 Dynamics of Laboratory Diapir and Plume Models. *J. Geophys. Res.* **80**, 705-717. (doi:10.1029/JB080i005p00705)
- [41] Whitehead, J. A. & Helfrich, K. R. 1986 The Korteweg-deVries equation from laboratory conduit and magma migration equations. *Geophys. Res. Lett.* **13**, 545-546. (doi:10.1029/GL013i006p00545)
- [42] Whitehead, J. A. & Helfrich, K. R. 1990 Magma waves and diapiric dynamics. In *Magma Transport and Storage* (ed M. P. Ryan), pp. 53-76. Chichester, UK: John Wiley & Sons.
- [43] Whitehead, J. A. & Helfrich, K. R. 1988 Wave transport of deep mantle material. *Nature* **336**, 59-61. (doi:10.1038/336059a0)
- [44] Whitham, G. B. 1965 A general approach to linear and non-linear dispersive waves using a Lagrangian. *J. Fluid Mech.* **22**, 273-283. (doi:10.1017/S0022112065000745)

- [45] Whitham, G. B. 1974 *Linear and nonlinear waves*. New York: Wiley.
- [46] Whitham, G. B. 1965 Non-linear dispersive waves. *Proc. Roy. Soc. Ser. A* **283**, 238-261.
- [47] Whitham, G. B. 1966 Nonlinear Dispersive Waves. *SIAM J. Appl. Math.* **14**, 956-958. (doi:10.1137/0114075)
- [48] Zakharov, V. E. & Ostrovsky, L. A. 2009 Modulation instability: the beginning. *Physica D* **238**, 540-548. (doi:10.1016/j.physd.2008.12.002)